JACS Au
AN OPEN ACCESS JOURNAL OF THE AMERICAN CHEMICAL SOCIETY

pubs.acs.org/jacsau
Article

Tailored Hollow Mesoporous Carbon Nanospheres from Soft Emulsions Enhance Kinetics in Sodium Batteries

Lu Liu, Sicheng Fan, Wendi Wang, Sixing Yin, Zirui Lv, Jie Zhang, Jingyu Zhang, Lanhao Yang, Yuzhu Ma, Qiulong Wei,* Dongyuan Zhao,* and Kun Lan*

Cite This: JACS Au 2024, 4, 2666−2675

Read Online

ACCESS | Metrics & More | Article Recommendations | Supporting Information

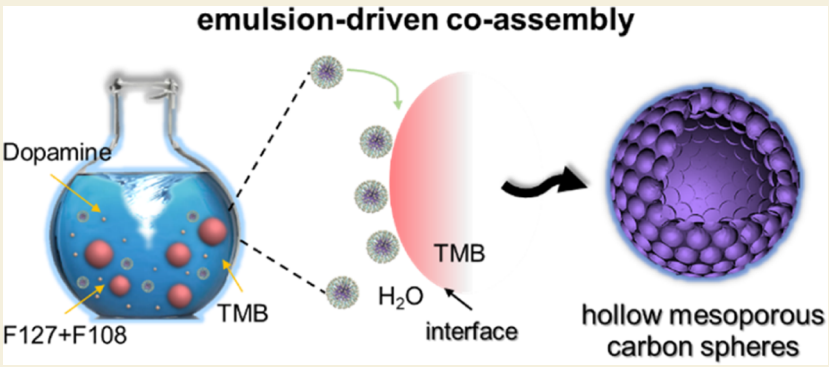

ABSTRACT: Mesoporous materials endowed with a hollow structure offer ample opportunities due to their integrated functionalities; however, current approaches mainly rely on the recruitment of solid rigid templates, and feasible strategies with better simplicity and tunability remain infertile. Here, we report a novel emulsion-driven coassembly method for constructing a highly tailored hollow architecture in mesoporous carbon, which can be completely processed on oil−water liquid interfaces instead of a solid rigid template. Such a facile and flexible methodology relies on the subtle employment of a 1,3,5-trimethylbenzene (TMB) additive, which acts as both an emulsion template and a swelling agent, leading to a compatible integration of oil droplets and composite micelles. The solution-based assembly process also shows high controllability, endowing the hollow carbon mesostructure with a uniform morphology of hundreds of nanometers and tunable cavities from 0 to 130 nm in diameter and porosities (mesopore sizes 2.5−7.7 nm; surface area 179−355 m^2 g^{-1}). Because of the unique features in permeability, diffusion, and surface access, the hollow mesoporous carbon nanospheres exhibit excellent high rate and cycling performances for sodium-ion storage. Our study reveals a cooperative assembly on the liquid interface, which could provide an alternative toolbox for constructing delicate mesostructures and complex hierarchies toward advanced technologies.

KEYWORDS: *mesoporous materials, nanoscience, hollow structure, soft template, sodium storage*

INTRODUCTION

Carbon materials with tailored nanoscopic configurations and nanopores have attracted increasing scientific interest because of their inherited exceptional properties and certain unconventional advantages,[1−5] thus rendering them promising as candidates in various applications such as catalysis, gas adsorption/separation, electrocatalysis, and electrochemical energy storage.[6−10] In particular, mesoporous carbon materials with a large pore size, high surface area, and tunable mesostructure offer considerable advantages in a variety of applications that involve efficient surface access and mass transfer.[11−16] Alternatively, the past decade also witnessed enormous endeavors in the structural control and optimization of hollow carbon structures with a low density to fully exploit their potential.[17−23] Nevertheless, it has been gradually acknowledged that mesopore channels are often not utilized thoroughly in a long diffusion length of bulk or micrometer-scale materials, while the excessive hollow architectures generally lead to unnecessary spatial occupation.[24−27] The rational combination of mesoscopic and hollow configurations could contribute to full-scale spatial utilization with retained permeability for further promotion in applied potentials. In this regard, a novel approach that enables one to precisely manipulate hollow voids in mesostructured carbon is highly

Received: May 11, 2024
Revised: June 21, 2024
Accepted: June 26, 2024
Published: July 2, 2024

https://doi.org/10.1021/jacsau.4c00421
JACS Au 2024, 4, 2666−2675

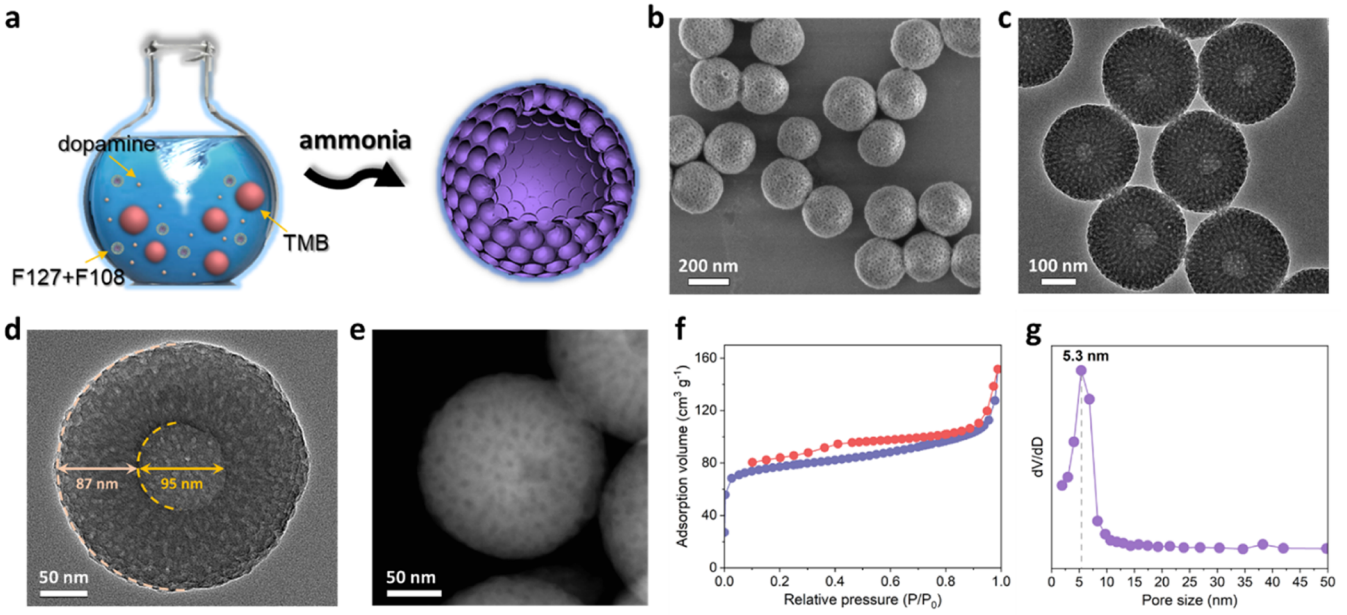

Figure 1. Synthesis and characterization of the ordered hollow mesoporous carbon nanospheres. (a) Scheme of the synthetic procedure for the hollow mesoporous carbon. Field-emission scanning electron microscopy (FESEM) image (b), transmission electron microscopy (TEM) images (c, d) at different magnifications, and high-angle annular dark-field scanning transmission electron microscopy (HAADF-STEM) image (e) of the hollow mesoporous carbon nanospheres. Nitrogen sorption isotherms (f) and correlated pore size distribution curve (g) for the hollow mesoporous carbon after calcination.

desirable for developing functional carbon structures with efficient mass diffusion and spatial occupation.

Currently, various approaches[18,24,25] have been at the forefront of efforts in molding hollow mesoporous carbon structures due to the advantageous combination of mesopores and hollow architectures. Among these strategies, using solid rigid particles as a core template represents a reliable pathway that has been used to fabricate a set of mesostructured shells with tunable compositions, mesopore channels, and thicknesses.[28−34] For example, Lou and co-workers reported a type of hollow mesoporous polydopamine nanospheres from the self-assembly of monolayered micelles on diverse functional materials.[29] Zhao et al. proposed a monomicelle interface-confined assembly strategy to precisely synthesize hollow mesoporous carbon superstructures with a monolayer of mesopores.[33] Although some progress has been made in hollow carbon mesostructures, such a hard-templating method still leads to drawbacks such as the inconvenience of multisteps, limited shell thickness, and undesired operation in nanoscale below 100 nm. On the other hand, other examples in soft-templating synthesis including emulsion[35,36] or vesicle-templating routes[37] are capable of processing micellar self-assembly on soft liquid matrixes such as emulsion droplets, vesicles, and gas bubbles, whereas such synergistic mesoscale and nanoscale assemblies on the liquid−liquid interface have met rare success.[38,39] Therefore, it is highly desired in further promote the assembly chemistry to fabricate hollow mesoporous carbon structures with better simplicity and tunability toward better potentials.

Herein, we present a novel emulsion-driven coassembly approach for the fabrication of uniform hollow mesoporous carbon nanospheres in hundreds of nanometers in a precise and controllable manner. These mesoporous carbons with a tailored hollow architecture can be assembled on the liquid emulsion template, which involves utilizing triblock copolymer Pluronic F127/F108/polydopamine micelles as building blocks and 1,3,5-trimethylbenzene (TMB) as an emulsion template. In this scenario, the TMB additive affords an emulsion interface for heterogeneous growth and can simultaneously be consumed as a swelling agent by interacting with amphiphilic micelles, which is the key to constructing highly tunable voids in carbon nanospheres. In consequence, a kind of ordered mesoporous carbon nanospheres with a high surface area of 263 m^2 g^{-1}, an open and uniform pore size of 5.3 nm, and a hollow void of ∼80 nm diameter can be synthesized through such a facile solution-processed method. Moreover, the assembly process enables one to realize accurate control of the void size from thin-shelled to entirely solid spheres, and the porosity associated with the mesopore size and surface area can also be manipulated by simply regulating the surfactant F127/F108 ratio or TMB content. Compared to solid mesoporous carbon and hard carbon, such an integration of the tunable mesoporosity and hollow cavity leads to significantly enhanced sodium-ion performance, including a high capacity of 210 mAh g^{-1} at 1C, a high rate capability up to 10C, and long-term cyclability (1600 cycles at 3C), as well as a high capacity retention of 88% at low temperatures (0 °C).

RESULTS AND DISCUSSION

Emulsion-Driven Coassembly

In the hard-templating approach, the only concern is regarding how to design a rational solid−liquid interface for moderate micelle assembly. Hollow mesoporous structures are generated after removing the solid cores, whereas the self-assembly from the soft template is rather difficult, which introduces more fundamental obstacles. The first key problem is to establish an encysted liquid−liquid interface for preferential micelle assembly at the exterior into the core−shell structure, as the liquid interface is difficult to stabilize compared to a solid template. Another constraint is to build appropriate interaction

https://doi.org/10.1021/jacsau.4c00421
JACS Au 2024, 4, 2666−2675

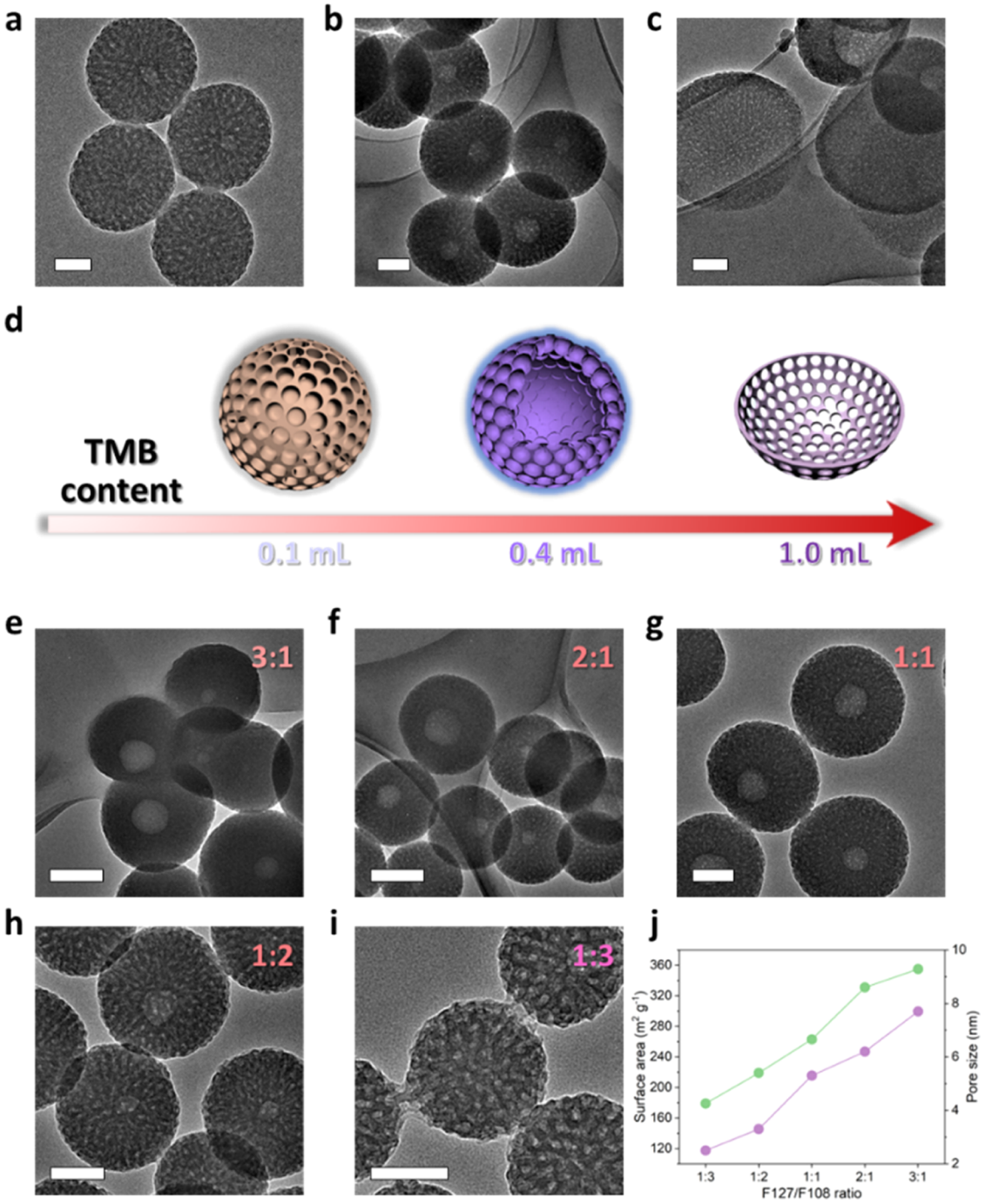

Figure 2. Systematic investigation of the assembly behavior. (a–d) TEM images of samples obtained using different TMB contents at (a) 0.1, (b) 0.4, and (c) 1.0 mL. (d) Structural models of products obtained at varied TMB contents. (e–i) TEM images of samples obtained by using different F108/F127 ratios from 3:1 to 1:3. (j) Plots of the surface area and pore size of samples with respect to the F127/F108 ratio. Scale bars are all 100 nm.

between the soft core template and the micelle for compatible interfacial assembly instead of homogeneous growth in solution, thereby leading to hollow mesostructures from the soft template being far out of reach.

In this work, we synthesize a kind of ordered mesoporous carbon nanospheres with uniform size and a well-regulated hollow architecture at the center via a proposed emulsion-driven coassembly strategy. To be specific, a biphasic solution containing the triblock copolymer F127/F108 as a building block, polydopamine as a carbon source, and TMB solvent as a core template was prepared and stirred at room temperature (Figure 1a). Noteworthily, the key in this protocol relies on the oily feature and swelling effect of the TMB solvent, which enables one to perform as an emulsion template in solution and bridge suitable interactions with composite micelles by hydrophobic affinity. After the addition of ammonia before the formation of the TMB/water biphasic solution within 30 min, the emulsion-encapsulated mesostructured carbon can be heterogeneously assembled on the oil–water interface during the moderate coassembly within 3 h, along with a transition

https://doi.org/10.1021/jacsau.4c00421
JACS Au 2024, 4, 2666–2675

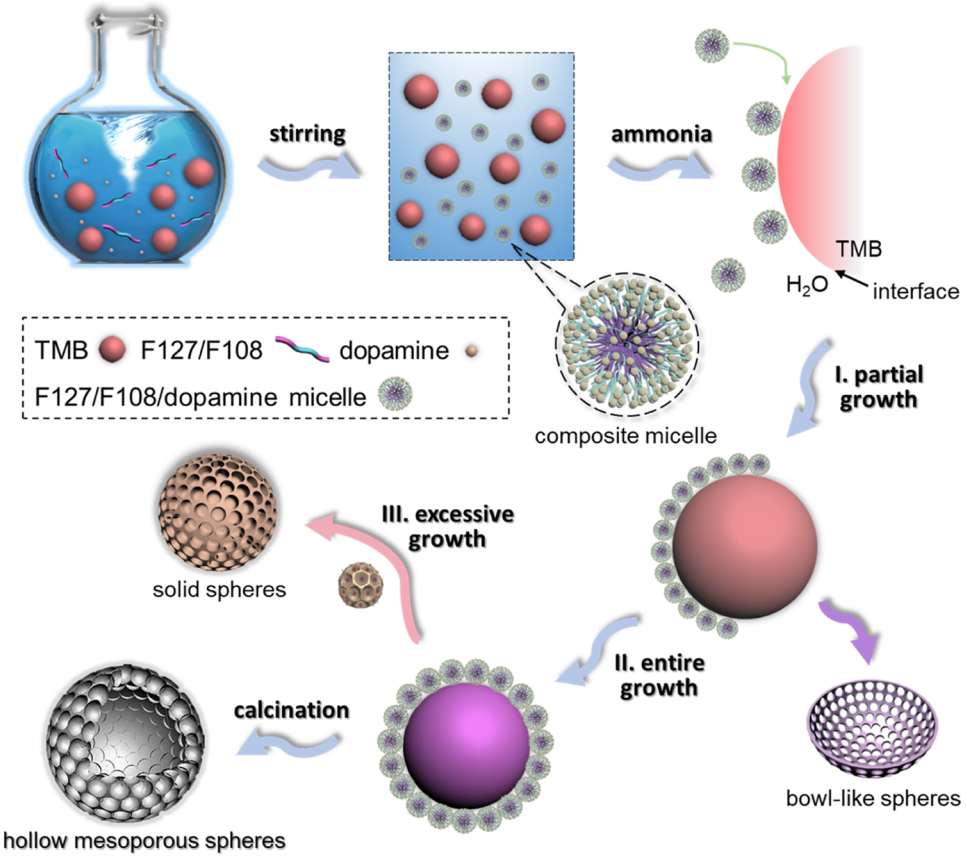

Figure 3. Schematic illustration of the ordered hollow mesoporous carbon through the emulsion-driven coassembly strategy. The assembly process involves three key steps. First, the composite micelles, composed of F127 and F108 as the inner core and dopamine as the exterior shell, are formed as building blocks in the TMB/water biphasic solution system. Then, due to the strong hydrophobic interaction between micelles and TMB droplets, the composite micelles start to aggregate on the liquid−liquid interface catalyzed by ammonia. Afterward, the continuous micelle growth undergoes a kinetics-dominated process from the exterior of TMB droplets, which leads to the intermediate formation of the bowl-like structure after partial growth, a hollow mesostructure after entire growth, and a solid structure after excessive growth. The hollow mesoporous carbon spheres are generated at last after calcination.

from a colorless suspension to a brown and black solution (Figure S1). After removing the soft TMB core and F127/F108 micelle template by centrifugation and calcination in a nitrogen atmosphere, the uniform hollow mesoporous carbon nanospheres with both a well-defined hollow cavity and mesoporosity can be generated at last.

Synthesis and Characterization

The ordered hollow mesoporous carbon nanospheres could be simply fabricated through the solution-processed assembly method (Figure S1). The large-scale and magnified field-emission scanning electron microscopy (FESEM) images show a uniform spherical morphology with an open mesoporous skeleton and a uniform diameter of around 240 nm for the fabricated products (Figures 1b and S2a). The mesoporous structure with a mean pore size of approximately 5 nm can be clearly visualized, along with a cavity of ∼95 nm in diameter in the interior (Figure 1c,1d). The well-defined hollow structure is also evidenced by the presence of holes within carbon spheres in the ultramicrotomed SEM image (Figure S2b). No lattice fringes and well-resolved diffraction rings can be observed in the high-resolution transmission electron microscopy (HRTEM) image and selected area electronic diffraction (SAED) pattern (Figure S3), indicating the amorphous characteristics of such mesoporous carbon after calcination in nitrogen at 1000 °C. Besides, elemental mapping images point out a uniform distribution of C, N, and O elements in the hollow mesoporous carbon spheres (Figures 1e and S4).

From nitrogen sorption measurements, the typical type IV isotherms with a hysteresis loop at P/P_0 = 0.2−0.8 and the centered pore size distribution at 5.3 nm indicate the well-defined mesoporous structure (Figure 1f,1g). The Brunauer−Emmett−Teller (BET) surface area and mesopore volume are calculated to be 263 $m^2\ g^{-1}$ and 0.23 $cm^3\ g^{-1}$, respectively. The nitrogen sorption may be caused by the incapability of nitrogen desorption in mesopores due to the shrinkage of soft carbon scaffolds and the presence of micropores.[40] In addition, the as-prepared hollow mesoporous carbon nanospheres undergo a weight loss of ∼48% after heating under a nitrogen atmosphere, mainly due to the decomposition of the F127/F108 template (Figure S5a). The Raman spectrum and X-ray diffraction (XRD) pattern exhibit typical peaks for characteristic hard carbon materials (Figure S5b,c), in good accordance with previous results.[41,42] The X-ray photoelectron spectroscopy (XPS) spectrum shows the presence of C, N, and O atoms, consistent with the elemental mapping results (Figure S6). The high-resolution C 1s spectrum exhibits three peaks at 284.9, 286.6, and 289.8 eV, as indexed to C═C, C−N, and O−C═O bonding states, respectively. The high-resolution N 1s spectrum can be deconvoluted into four peaks at 398.4,

https://doi.org/10.1021/jacsau.4c00421
JACS Au 2024, 4, 2666−2675

399.8, 400.7, and 402.1 eV, which can be assigned to N-6, N-5, N-G, and N−O bonding states, respectively.[15,16]

Manipulation of the Assembly Process

In order to underscore the essential role of TMB droplets, control experiments without the TMB additive were conducted. The observed random and solid carbon spheres imply that the TMB solvent directly determines the presence of hollow architectures by facilitating the formation of uniform nanoscale emulsions as a soft template (Figure S7). To further validate this hypothesis, systematic regulation of the amount of TMB from 0.1 to 1.0 mL was carried out, showing a gradual transformation from solid, hollow, to bowl-like mesostructured carbon spheres with an increase in the TMB amount (Figures 2a−d and S8). This response clearly supports the fact that the hollow configuration can be modified and originates from TMB droplets at an appropriate region of water/oil ratio. Besides, excessive oil phase in the system could cause unstable emulsion formation, thereby generating uneven distribution of droplets and incomplete growth into nanobowls. As the TMB amount increases, dynamic light scattering (DLS) analyses of TMB and TMB/F127/F108 solutions exhibit increased size distributions of the gradually opaque solutions, which implies the appearance of ultralarge, nonuniform emulsion droplets (Figure S9), congruent with the previous phenomenon.

Apart from the tunable hollow structure, another discovery garnered from this strategy is that the porosity and nanoscopic cavity could be controlled by varying the F127/F108 template ratio. At an F127/F108 ratio of 3:1, the generated cavities in the center are much larger but less uniform (Figure 2e). A gradual increase in the F127/F108 ratio leads to a declined hollow structure, while the sizes of mesoporous carbon nanospheres are negligibly changed (Figures 2f−i and S10). When the ratio reaches 1:3, the solid mesoporous carbon nanospheres are formed with an obviously enhanced mesopore size (Figure S11), implying that the TMB content, which serves as the droplet template, is transformed into a swelling agent to generate larger F127/F108/TMB/dopamine composite micelles. From the nitrogen sorption results of these five samples, the mesopore size gradually increases from 2.5 to 7.7 nm, and the surface area also exhibits an increasing tendency from 179 to 355 $m^2\ g^{-1}$, indicative of the highly tailored porosity of such an approach (Figures 2j and S12, Table S1). A high F127 ratio leads to a larger mesopore size, while a higher F108 ratio allows for retaining a hollow architecture. We conclude that such a regulation based on the template ratio is possibly ascribed to the varied hydrophobic affinity toward TMB due to the different hydrophobic/hydrophilic segments of F127 and F108 copolymers.[15,43]

Ex situ intermediate observations at different time intervals were also investigated to gain insights into the assembly process. As visualized in the TEM and SEM results, the emulsion-driven coassembly process involves the gradual transformation from bowl-like spheres at 0.5 h, eccentric hollow spheres at 1 h, and hollow spheres with declined cavity at 2 and 3 h, respectively (Figure S13a−d). This phenomenon reveals an atypical growth process initiated from the exterior region instead of heterogeneous growth on the solid template from the interior, which suggests that the TMB droplets as a core template are swallowed and consumed with continuous micelle assembly on the liquid−oil interface (Figure S13e). After reaction for over 5 h, the solid mesoporous spheres are observed, further validating the depletion of TMB droplets by hydrophobic interaction between the oily TMB and F127/F108 copolymers (Figure S14). In addition, to probe other impactors that might affect the formation of TMB droplets, control experiments under different stirring rates were also conducted. The products display almost similar hollow mesoporous structures, demonstrating that the stirring rate at a proper region has a minor influence on the assembly behavior (Figure S15).

Assembly Mechanism

On the basis of the above observations, we propose an emulsion-driven coassembly mechanism for the formation of such hollow mesoporous carbon nanospheres (Figure 3). First, the water/ethanol solution system is prepared with dopamine as the carbon source and the triblock copolymer of F127 and F108 as the micelle template. With the addition of the oil-phase TMB solvent, the aqueous solution turns into an oil-in-water system, and the F127/F108/TMB/dopamine composite micelles are generated as a building block for the mesostructure. Noteworthily, the TMB solvent serves not only as a swelling agent for F127/F108 micelles to form a large mesopore size but also as a liquid core template for micelle assembly at the oil−water interface into core−shell structured nanospheres. This is the key point for the successful construction of such hollow mesoporous structures by bridging connections between the micelle self-assembly and heterogeneous growth on the liquid−liquid interface. Subsequently, during the assembly triggered by ammonia, these preformed F127/F108/TMB/dopamine composite micelles are inclined to heterogeneously assemble on the oil−water interface rather than undergo self-aggregation due to the strong hydrophobic interactions between the composite micelles and oily TMB droplets. With continuous assembly, the carbon shell thickens. Because of the swelling effect of TMB, the continuously gathered composite micelles at the shell of droplets tend to gradually encompass and consume these large TMB droplets, thus leading to a core−shell structure (TMB droplet@composite micelle) at last. The final hollow mesoporous carbon nanospheres with a uniform diameter and an enlarged mesopore size can be finally fabricated after removing the TMB and F127/F108 templates by simply washing and calcination.

As the F127/F108/polydopamine composite micelles can interact with large TMB droplets due to the strong affinity of the hydrophobic PPO segment, such a solution-processed assembly route endows them with a delicately tailored nanoscopic architecture by tuning the TMB amount or reaction time, leading to a bowl-like structure in primary growth and solid mesoporous spheres after emulsion exhaustion. Moreover, the position of the oily TMB solvent can also be monitored by controlling the hydrophobic affinity with copolymers. In these two copolymers with varied hydrophile lipophilic balance (HLB) values, the copolymer F127 possesses more hydrophobic segments than F108 (hydrophobic/hydrophilic ratio R_{F127} = 0.66, R_{F108} = 0.38). Thus, a higher F127/F108 ratio results in an enlarged mesopore size by swelling more TMB into the composite micelle, while a lower ratio gives rise to a weakened swelling effect, and the hollow voids derived from TMB droplets are much magnified.

Electrochemical Sodium Storage

To demonstrate the potential of the hollow mesoporous carbon (hollow meso-carbon) anode, its electrochemical

https://doi.org/10.1021/jacsau.4c00421
JACS Au 2024, 4, 2666−2675

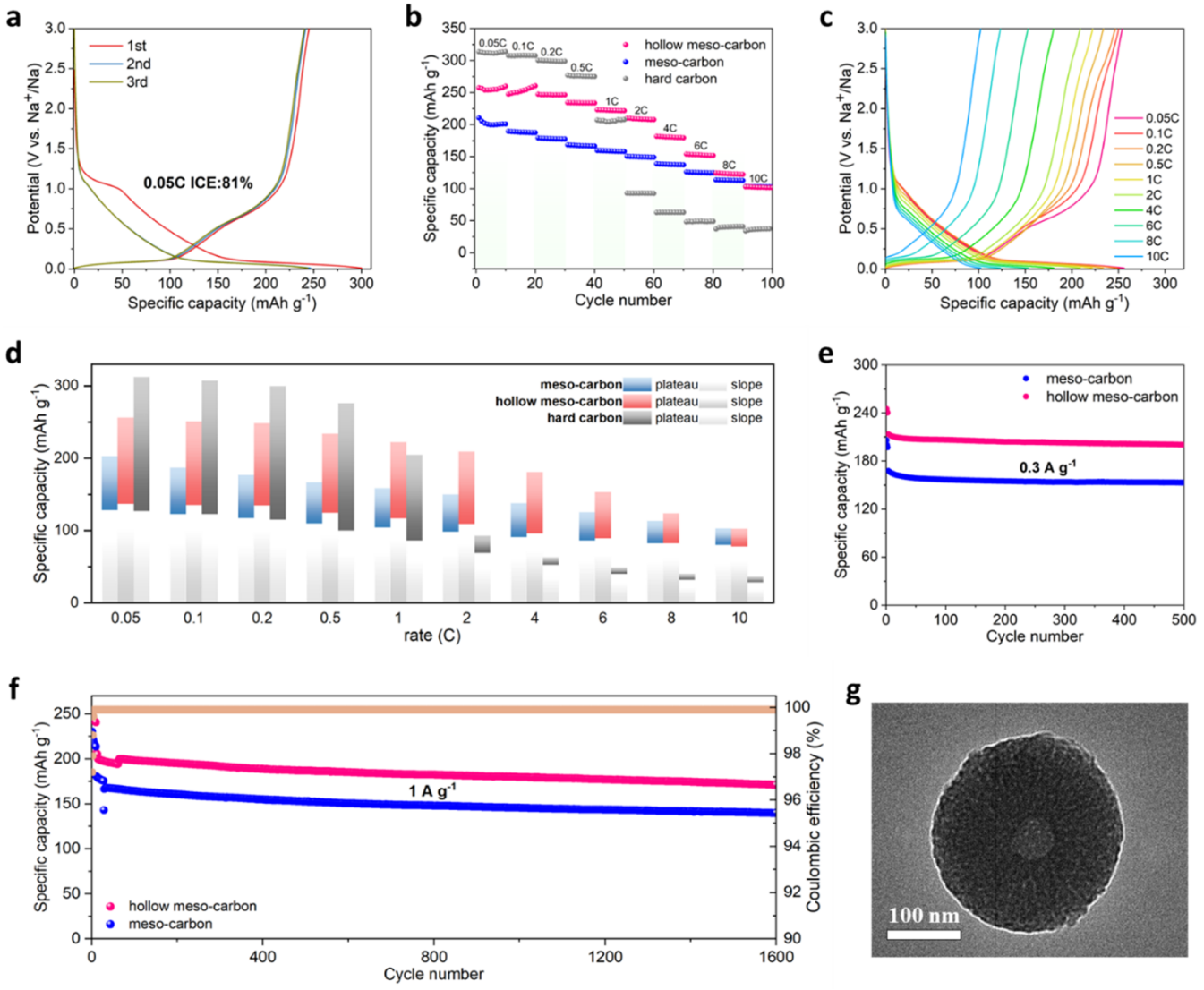

Figure 4. Sodium storage performances of the hollow mesoporous carbon nanospheres. (a) Charge−discharge profiles of the initial three cycles of the hollow meso-carbon at 0.05C. (b) Rate performances ramping from 0.05 to 10C of the hollow meso-carbon compared with meso-carbon and hard carbon electrodes. (c) Galvanostatic charge−discharge curves at current densities from 0.05 to 10C for the hollow meso-carbon. (d) Separation of the capacity from the plateau and slope for the hollow meso-carbon, meso-carbon, and hard carbon electrodes at varied rates from 0.05 to 10C. (e, f) Cycling stability of the hollow meso-carbon and meso-carbon after 500 charge−discharge cycles at 1C (e) and after 1600 charge−discharge cycles at 3C (f). (g) TEM image of the hollow meso-carbon nanospheres after 1600 cycles at 1 A g^{-1}.

sodium-ion storage was incorporated using previous methods[44,45] in comparison to solid mesoporous carbon spheres (meso-carbon) and commercial hard carbon. The galvanostatic charge−discharge profiles during the initial three cycles at 0.05C exhibit a typical slope region above 0.1 V and a plateau region below 0.1 V (Figure 4a). The hollow meso-carbon electrode delivers an initial sodiated/desodiated capacity of 295/240 mAh g^{-1}, corresponding to an initial Coulombic efficiency (ICE) of 81%, which is higher than the 263/203 mAh g^{-1} of the meso-carbon with ICE of 77% (Figure S16a,b). The reversible capacity of hollow meso-carbon is rapidly stabilized at 248 mAh g^{-1} in the third cycle, higher than that of meso-carbon. Besides, the compact density of the hollow meso-carbon is comparable to that of hard carbon (Figure S17), thus ensuring that the hollow mesoporous structure does not compromise the overall volumetric energy density.

The rate capacities of the three electrodes were further measured. The hollow meso-carbon displays higher capacities than those of the meso-carbon at each rate from 0.05 to 10C (Figure 4b). Although the hard carbon displays a higher capacity at low rates, the lack of an open porous structure with fast Na^+ transmission channels leads to a poor rate performance, which leads to a rapid capacity decay at 1C. Galvanostatic charge−discharge curves at current densities from 0.05 to 10C further imply the high rate capability of the hollow meso-carbon compared to meso-carbon and hard carbon (Figures 4c and S16c,d), revealing the rapid ion transport in mesoporous channels with small potential polarizations. Figure 4d distinguishes the charge storage contributions from different slope and plateau regions according to charge−discharge curves. It is noted that the capacity from the plateau region of the hollow meso-carbon is higher than that of the meso-carbon at each current. With an increase in the charge−discharge rate, the plateau capacities of the meso-carbon anode fade due to the polarization but are retained proportionally, whereas there is no apparent plateau

https://doi.org/10.1021/jacsau.4c00421
JACS Au 2024, 4, 2666−2675

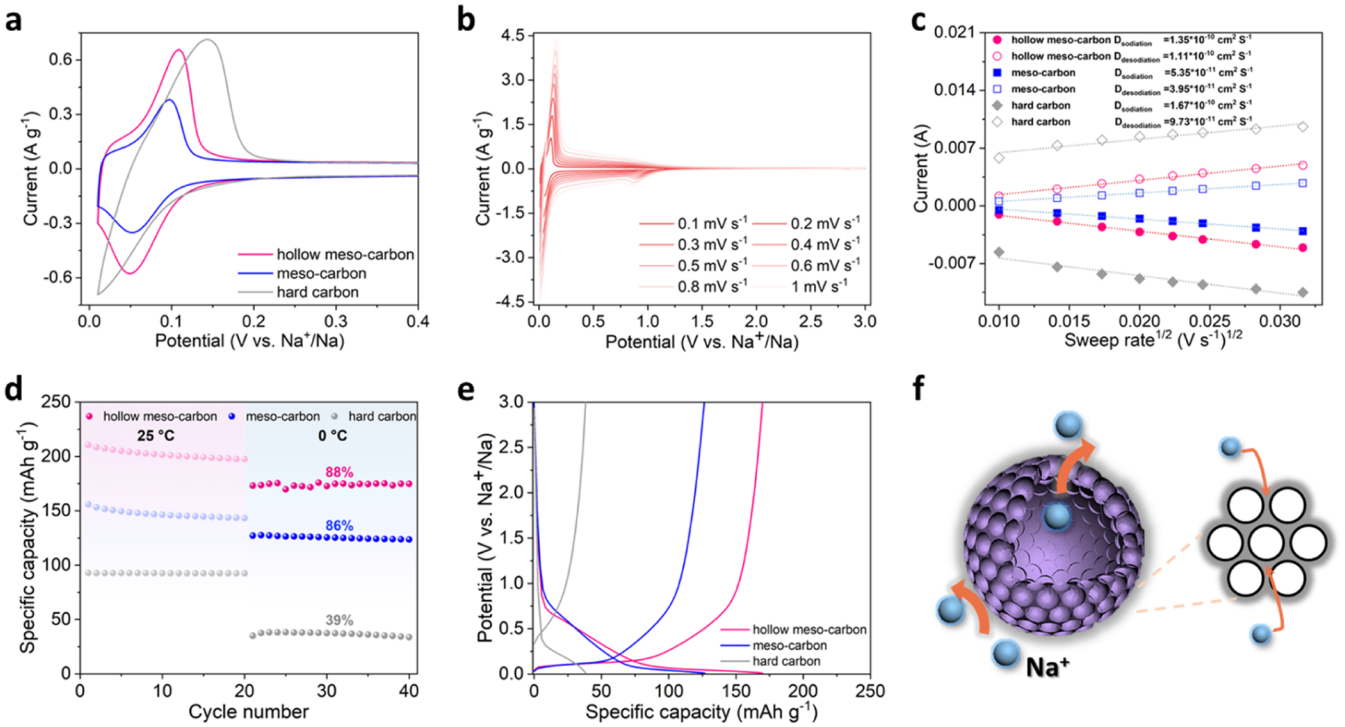

Figure 5. Dynamic study and low-temperature performances. (a) CV curves for the three samples at a scan rate of 1 mV s^{-1}. (b) CV curves for the hollow meso-carbon at various scan rates from 0.1 to 1.0 mV s^{-1}. (c) Plots of current versus scan $rate^{-1/2}$ of the three electrodes to calculate the diffusion coefficient. (d) Capacity comparison for the three samples at 3C conducted at room temperature and 0 °C, respectively. (e) Charge–discharge profiles for the three samples at 3C conducted at 0 °C. (f) Schematic model of the hollow meso-carbon, showing the charge storage mechanism.

contribution of the hard carbon over 2C, demonstrating the high rate performance. From the long-term cycling stability measured at 1C, the hollow meso-carbon anode displays reversible capacities of 195 mAh g^{-1} after 500 cycles without noticeable decay (a retention of 93%), much higher than that of the meso-carbon with a retention of 89% (Figure 4e). The corresponding capacity retention of the hollow meso-carbon is 88%. At a higher rate of 1 A g^{-1}, the reversible capacities of 171 mAh g^{-1} with a retention of 83% after 1600 cycles are achieved for the hollow meso-carbon, and the Coulombic efficiency is kept at over 99% for each cycle (Figure 4f), suggesting the significance of the hollow mesostructure for realizing excellent cyclability. Furthermore, the hollow and mesoporous architecture show negligible changes after long-term cycling, further demonstrating the excellent reversibility of such a hollow mesoporous carbon (Figures 4g and S18).

Dynamic Study and Material Design Implications

To gain further insights into charge storage, cyclic voltammetry (CV) was performed to investigate the sodium-ion storage kinetics. The three carbon materials exhibit a pair of sharp peaks located at the potential region of 0.2–0.01 V vs Na^+/Na (Figure S19a–c), corresponding to the low potential plateau in the charge–discharge profiles. The magnified CV curve (Figure 5a) shows smaller polarizations of the hollow meso-carbon and meso-carbon than that of the hard carbon, indicating the enhanced reaction kinetics of the open porous structure. The CV curves display similar peaks with gradually increased currents when increasing scan rates (Figures 5b and S19d,e). The peak shifts of the hollow meso-carbon and meso-carbon are much alleviated compared to that of the hard carbon, indicating the promoted kinetics for ionic diffusion. The diffusion coefficient based on the sodiation and desodiation of the hollow meso-carbon is calculated to be 1.35×10^{-10} and 1.11×10^{-10} cm^{-2} S^{1-}, higher than those of meso-carbon and hard carbon (Figure 5c), further demonstrating the enhanced charge kinetics in the hollow mesostructure. The low-temperature charge–discharge performances were further evaluated to demonstrate the potential of hollow meso-carbon. As shown in Figure 5d, the hollow meso-carbon can achieve a higher specific capacity of 170 mAh g^{-1} at 3C and 0 °C, corresponding to a capacity retention of 88% compared to that at room temperature. The rapid diffusion of solvated Na^+ ions in the hollow mesoporous channels facilitates the "intercalation-fill" reaction for the plateau region (Figure 5e). However, the commercial hard-carbon anode could not be well charged and discharged at 0 °C due to the unsatisfactory kinetics of long-term diffusion of Na^+ in hard carbon.

There are two features of the hollow mesoporous carbon that exert enhanced electrochemical sodium storage. The first characteristic is the moderately sized cavity. The appropriate hollow structure enables the maintenance of structural integrity during cycling and simultaneously possesses comparable spatial occupation with solid nanospheres, as evidenced by the negligible decline of the compact density to meso-carbon (Figure S20). The second is the well-defined mesoscopic structure with a highly regulated porosity. The opened and ordered mesopore channel benefits comprehensive electrolyte access and rapid reversible redox reactions, which favors pore-filling-dominated charge storage and determines excellent electrochemical behavior at high rates (Figure 5f).[46,47] The stably retained hollow and mesoporous structure after long-term cycles further validates the excellent reversibility of hollow mesoporous carbon. Our designed material provides a

https://doi.org/10.1021/jacsau.4c00421
JACS Au 2024, 4, 2666–2675

reliable model system with both boosted plateau charge storage and diffusion kinetics, thus allowing for enhanced electrochemical sodium storage.

CONCLUSIONS

In summary, a kind of uniform and ordered hollow mesoporous carbon nanospheres with high controllability over the shell thickness and mesochannels were fabricated. The success of such a novel hollow carbon mesostructure relies on an ingenious micelle assembly incorporated with TMB emulsions, which requires no solid substrates as a hard template. In this emulsion-driven coassembly process, TMB not only performs as a swelling agent to enrich the mesopore size of F127/polydopamine micelles but also provides a nanoscale liquid template to direct the interfacial micelle self-assembly into uniform spherical morphology. The resultant hollow mesoporous carbon nanospheres show a uniform size at ∼240 nm with tailored cavities from 0 to 130 nm in diameter, mesopore sizes from 2.5 to 7.7 nm, and surface areas from 179 to 355 $m^2 g^{-1}$. The incorporated anode using this material with both hollow and mesoporous structures for boosted pore filling and mass diffusion enables enhanced performances in sodium storage, including a high reversible capacity of 295 mAh g^{-1}, a rate capability up to 10C, long-term cycling over 1600 cycles at 3C, and high retention (88%) at a low temperature of 0 °C. This study underscores a better and alternative pathway for designing hollow mesostructures from facile solution-processed assembly chemistry, as well as an advanced model platform toward effective sodium storage in the future.

EXPERIMENTAL SECTION

Chemicals

Triblock poly(ethylene oxide)-*b*-poly(propylene oxide)-*b*-poly(ethylene oxide) Pluronic F127 (M_{av} = 12,700) and F108 (M_{av} = 14,600) were purchased from Sigma-Aldrich. Dopamine hydrochloride was purchased from Aladdin. 1,3,5-Trimethylbenzene (TMB), ammonia solution (25−28%), and anhydrous ethanol (AR, ≥99.7%) were provided by Shanghai Chemical Reagent. All chemicals were used as received without further purification. Deionized water was used in all experiments.

Material Characterizations

Transmission electron microscopy (TEM) and high-resolution transmission electron microscopy (HRTEM) were performed using a JEM-2100F microscope (JEOL, Japan) operated at 200 kV. Field-emission scanning electron microscopy (FESEM) images were observed on a Gemini Ultra55 (Zeiss). Samples for TEM and FESEM analyses were prepared by adding a drop of the dispersion in ethanol on copper grids and silicon substrates. Nitrogen adsorption−desorption measurements were performed at 77 K with an ASAP 2420 and Micromeritics Tristar 3020 analyzer. Dynamic light scattering (DLS) and ζ-potential experiments were performed on a Malvern Zetasizer 3600 (Malvern Instruments). X-ray diffraction (XRD) patterns of samples were collected by using a Bruker D8 powder X-ray diffractometer (Germany) with Cu Ka radiation (40 kV, 40 mA). X-ray photoelectron spectroscopy (XPS) results were collected by using an AXIS ULTRA DLD XPS System with MONO Al source (Shimadzu Corp.). Photoelectron spectrometry was recorded using monochromatic Al KR radiation under vacuum at 5×10^{-9} Pa. All binding energies were referenced to the C 1s peak at 284.6 eV of the surface adventitious carbon. The Raman spectra of samples were obtained by using a Raman system (HORIBA micro) with a laser excitation wavelength of 532 nm.

Synthesis of the Hollow Mesoporous Carbon Nanospheres

The hollow mesostructured carbon was fabricated according to the emulsion-driven assembly approach. In a typical synthesis, 0.1 g of F108 and 0.1 g of F127 are respectively dispersed in 5 mL of ethanol by ultrasonication until the solutions become clear. Then, the above solutions are mixed with 10 mL of H_2O, 0.1 g of DA, 0.4 mL of TMB, under stirring 30 min (500 rpm). After that, 1 mL of ammonia is quickly added to the reaction mixture under stirring (350 rpm). The product is collected by centrifugation after 3 h and then washed with water and ethanol several times. To prepare hollow mesostructured carbon, the obtained product is heated at 1 °C min^{-1} from room temperature to 350 °C and kept at this temperature for 3 h under a nitrogen atmosphere. The temperature is then further increased at 1 °C min^{-1} to 1000 °C and kept at this temperature for 2 h. To systematically investigate this assembly chemistry, a series of control experiments were carried out by replacing or changing factors that have significant influence on such an emulsion-driven coassembly: (1) change in the ratio of F108/F127: 1/3, 1/2, 2/1, and 3/1; (2) change in the amount of TMB: 0.1, 0.2, 0.4, 0.6, 0.8, and 1.0 mL; (3) change in the reaction time: 0.5, 1, 2, 3, and 5 h.

Electrochemical Measurements

The electrodes were prepared by mixing the active material, conductive carbon black (Ketjen Black, EC-600JD), carboxymethyl cellulose (CMC) binder, and styrene−butadiene rubber (SBR) in a weight ratio of 90:5:3:2. The slurry was cast onto a copper foil and dried at 80 °C in a vacuum oven for 12 h. The active material mass loading was 1.5−2.0 mg cm^{-2}. 2032-Type coin cells, using active materials as the working electrode, a sodium foil as the counter and reference electrodes, and a glass fiber separator (Whatman, GF/C) saturated with 1.0 M NaPF6 in diethylene glycol dimethyl ether as the electrolyte, were assembled in argon-filled glove boxes. All of the electrochemical tests were undertaken on an electrochemical workstation (Bio-Logic VMP3) at room temperature. Discharge−charge tests for electrodes were carried out with a duration of 0.6 h and a rest time of another 0.5 h for each step. *Ex situ* TEM images and XRD patterns were obtained by disassembling the cycled coin cells in a groove box and washing them with the solvent.

ASSOCIATED CONTENT

Supporting Information

The Supporting Information is available free of charge at https://pubs.acs.org/doi/10.1021/jacsau.4c00421.

Additional experimental details for the preparation, characterization of materials, and electrochemical measurements (Figures S1−S20 and Tables S1−S2) (PDF)

Mesoporous materials endowed with hollow structure offer ample opportunities due to their integrated functionalities, however, current approaches mainly rely on recruitment of solid rigid templates, and feasible strategies with better simplicity and tunability remain infertile (PDF)

AUTHOR INFORMATION

Corresponding Authors

Qiulong Wei − *Department of Material Science and Engineering, Xiamen University, Xiamen 361005, P. R. China;* orcid.org/0000-0002-9551-8309; Email: qlwei@xmu.edu.cn

Dongyuan Zhao − *College of Chemistry and Materials, Department of Chemistry, Laboratory of Advanced Materials, Fudan University, Shanghai 200433, P. R. China; College of Energy Materials and Chemistry, College of Chemistry and Chemical Engineering, Inner Mongolia University, Hohhot*

https://doi.org/10.1021/jacsau.4c00421
JACS Au 2024, 4, 2666−2675

010070, P. R. China; orcid.org/0000-0001-8440-6902; Email: dyzhao@fudan.edu.cn

Kun Lan − *College of Energy Materials and Chemistry, College of Chemistry and Chemical Engineering, Inner Mongolia University, Hohhot 010070, P. R. China;* orcid.org/0000-0001-8983-0155; Email: k_lan@imu.edu.cn

Authors

Lu Liu − *College of Chemistry and Materials, Department of Chemistry, Laboratory of Advanced Materials, Fudan University, Shanghai 200433, P. R. China*

Sicheng Fan − *Department of Material Science and Engineering, Xiamen University, Xiamen 361005, P. R. China*

Wendi Wang − *College of Energy Materials and Chemistry, College of Chemistry and Chemical Engineering, Inner Mongolia University, Hohhot 010070, P. R. China*

Sixing Yin − *College of Chemistry and Materials, Department of Chemistry, Laboratory of Advanced Materials, Fudan University, Shanghai 200433, P. R. China*

Zirui Lv − *College of Chemistry and Materials, Department of Chemistry, Laboratory of Advanced Materials, Fudan University, Shanghai 200433, P. R. China*

Jie Zhang − *College of Chemistry and Materials, Department of Chemistry, Laboratory of Advanced Materials, Fudan University, Shanghai 200433, P. R. China*

Jingyu Zhang − *College of Energy Materials and Chemistry, College of Chemistry and Chemical Engineering, Inner Mongolia University, Hohhot 010070, P. R. China*

Lanhao Yang − *College of Energy Materials and Chemistry, College of Chemistry and Chemical Engineering, Inner Mongolia University, Hohhot 010070, P. R. China*

Yuzhu Ma − *College of Energy Materials and Chemistry, College of Chemistry and Chemical Engineering, Inner Mongolia University, Hohhot 010070, P. R. China*

Complete contact information is available at: https://pubs.acs.org/10.1021/jacsau.4c00421

Notes

The authors declare no competing financial interest.

■ ACKNOWLEDGMENTS

This work was supported by the National Key R&D Program of China (2024YFE0101100), the National Natural Science Foundation of China (22205118 and 22375108), the Young Talents of Science and Technology of Inner Mongolia (NJYT23037), the Natural Science Foundation of Inner Mongolia (2023JQ06), the Grassland Talent Program of Inner Mongolia, and the "Junma" Program of Inner Mongolia University. Q.W. acknowledges support from the National Natural Science Foundation of China (22179113) and the Science and Technology Projects of Innovation Laboratory of Energy Materials of Fujian Province (HRTP-2022-19).

■ REFERENCES

(1) Roberts, A. D.; Li, X.; Zhang, H. Porous carbon spheres and monoliths: morphology control, pore size tuning and their applications as Li-ion battery anode materials. *Chem. Soc. Rev.* **2014**, *43*, 4341−4356.

(2) Wang, H.; Shao, Y.; Mei, S.; Lu, Y.; Zhang, M.; Sun, J.; Matyjaszewski, K.; Antonietti, M.; Yuan, J. Polymer-derived heteroatom-doped porous carbon materials. *Chem. Rev.* **2020**, *120*, 9363−9419.

(3) Moreno, C.; Vilas-Varela, M.; Kretz, B.; Garcia-Lekue, A.; Costache, M. V.; Paradinas, M.; Panighel, M.; Ceballos, G.; Valenzuela, S. O.; Peña, D.; Mugarza, A. Bottom-up synthesis of multifunctional nanoporous graphene. *Science* **2018**, *360*, 199−203.

(4) Tang, J.; Salunkhe, R. R.; Liu, J.; Torad, N. L.; Imura, M.; Furukawa, S.; Yamauchi, Y. Thermal conversion of core-shell metal-organic frameworks: a new method for selectively functionalized nanoporous hybrid carbon. *J. Am. Chem. Soc.* **2015**, *137*, 1572−1580.

(5) Bin, D. S.; Chi, Z. X.; Li, Y.; Zhang, K.; Yang, X.; Sun, Y. G.; Piao, J. Y.; Cao, A. M.; Wan, L. J. Controlling the compositional chemistry in single nanoparticles for functional hollow carbon nanospheres. *J. Am. Chem. Soc.* **2017**, *139*, 13492−13498.

(6) Liu, J.; Wickramaratne, N. P.; Qiao, S.; Jaroniec, M. Molecular-based design and emerging applications of nanoporous carbon spheres. *Nat. Mater.* **2015**, *14*, 763−774.

(7) Zhang, J.; Qu, L.; Shi, G.; Liu, J.; Chen, J.; Dai, L. N, P-codoped carbon networks as efficient metal-free bifunctional catalysts for oxygen reduction and hydrogen evolution reactions. *Angew. Chem., Int. Ed.* **2016**, *128*, 2270−2274.

(8) Tian, H.; Liang, J.; Liu, J. Nanoengineering carbon spheres as nanoreactors for sustainable energy applications. *Adv. Mater.* **2019**, *31*, No. 1903886.

(9) Mo, R.; Li, F.; Tan, X.; Xu, P.; Tao, R.; Shen, G.; Lu, X.; Liu, F.; Shen, L.; Xu, B.; Xiao, Q.; Wang, X.; Wang, C.; Li, J.; Wang, G.; Lu, Y. High-quality mesoporous graphene particles as high-energy and fast-charging anodes for lithium-ion batteries. *Nat. Commun.* **2019**, *10*, No. 1474.

(10) Han, F.; Qian, O.; Meng, G.; Lin, D.; Chen, G.; Zhang, S.; Pan, Q.; Zhang, X.; Zhu, X.; Wei, B. Structurally integrated 3D carbon tube grid-based high-performance filter capacitor. *Science* **2022**, *377*, 1004−1007.

(11) Benzigar, M. R.; Talapaneni, S. N.; Joseph, S.; Ramadass, K.; Singh, G.; Scaranto, J.; Ravon, U.; Al-Bahily, K.; VinuBenzigar, A. Recent advances in functionalized micro and mesoporous carbon materials: synthesis and applications. *Chem. Soc. Rev.* **2018**, *47*, 2680−2721.

(12) Zhao, T.; Chen, L.; Lin, R.; Zhang, P.; Lan, K.; Zhang, W.; Li, X.; Zhao, D. Interfacial assembly directed unique mesoporous architectures: from symmetric to asymmetric. *Acc. Mater. Res.* **2020**, *1*, 100−114.

(13) Fang, Y.; Gu, D.; Zou, Y.; Wu, Z.; Li, F.; Che, R.; Deng, Y.; Tu, B.; Zhao, D. A low-concentration hydrothermal synthesis of biocompatible ordered mesoporous carbon nanospheres with tunable and uniform size. *Angew. Chem., Int. Ed.* **2010**, *49*, 7987−7991.

(14) Guan, B. Y.; Yu, L.; Lou, X. Formation of asymmetric bowl-like mesoporous particles via emulsion-induced interface anisotropic assembly. *J. Am. Chem. Soc.* **2016**, *138*, 11306−11311.

(15) Peng, L.; Peng, H.; Liu, Y.; Wang, X.; Hung, C.; Zhao, Z.; Chen, G.; Li, W.; Mai, L.; Zhao, D. Spiral self-assembly of lamellar micelles into multi-shelled hollow nanospheres with unique chiral architecture. *Sci. Adv.* **2021**, *7*, No. eabi7403.

(16) Peng, L.; Peng, H.; Xu, L.; Wang, B.; Lan, K.; Zhao, T.; Che, R.; Li, W.; Zhao, D. Anisotropic self-assembly of asymmetric mesoporous hemispheres with tunable pore structures at liquid-liquid interfaces. *J. Am. Chem. Soc.* **2022**, *144*, 15754−15763.

(17) Xu, X.; Zhang, Z.; Wang, X. Well-defined metal-organic-framework hollow nanostructures for catalytic reactions involving gases. *Adv. Mater.* **2015**, *27*, 5365−5371.

(18) Wang, X.; Feng, J.; Bai, Y.; Zhang, Q.; Yin, Y. Synthesis, properties, and applications of hollow micro-/nanostructures. *Chem. Rev.* **2016**, *116*, 10983−11060.

(19) Sun, L.; Lv, H.; Feng, J.; Guselnikova, O.; Wang, Y.; Yamauchi, Y.; Liu, B. Noble-metal-based hollow mesoporous nanoparticles: synthesis strategies and applications. *Adv. Mater.* **2022**, *34*, No. 2201954.

(20) Zheng, G.; Lee, S. W.; Liang, Z.; Lee, H.; Yan, K.; Yao, H.; Wang, H.; Li, W.; Chu, S.; Cui, Y. Interconnected hollow carbon nanospheres for stable lithium metal anodes. *Nat. Nanotechnol.* **2014**, *9*, 618−623.

(21) Zeng, R.; Lian, K.; Su, B.; Lu, L.; Lin, J.; Tang, D.; Lin, S.; Wang, X. Versatile synthesis of hollow metal sulfides via reverse cation exchange reactions for photocatalytic CO_2 reduction. *Angew. Chem., Int. Ed.* **2021**, *60*, 25055−25062.
(22) Fang, Y.; Luan, D.; Gao, S.; Lou, X. Rational design and engineering of one-dimensional hollow nanostructures for efficient electrochemical energy storage. *Angew. Chem., Int. Ed.* **2021**, *60*, 20102−20118.
(23) Kim, S. M.; Jeon, M.; Kim, K. W.; Park, J.; Lee, I. S. Postsynthetic functionalization of a hollow silica nanoreactor with manganese oxide-immobilized metal nanocrystals inside the cavity. *J. Am. Chem. Soc.* **2013**, *135*, 15714−15717.
(24) Li, Y.; Shi, J. Hollow-structured mesoporous materials: chemical synthesis, functionalization and applications. *Adv. Mater.* **2014**, *26*, 3176−3205.
(25) Teng, Z.; Li, W.; Tang, Y.; Elzatahry, A.; Lu, G.; Zhao, D. Mesoporous organosilica hollow nanoparticles: synthesis and applications. *Adv. Mater.* **2019**, *31*, No. 1707612.
(26) Xia, Y.; Mathis, T. S.; Zhao, M.; Anasori, B.; Dang, A.; Zhou, Z.; Cho, H.; Gogotsi, Y.; Yang, S. Thickness-independent capacitance of vertically aligned liquid-crystalline MXenes. *Nature* **2018**, *557*, 409−412.
(27) Falcaro, P.; Okada, K.; Hara, T.; Ikigaki, K.; Tokudome, Y.; Thornto, A. W.; Hill, A. J.; Williams, T.; Doonan, C.; Takahashi, M. Centimetre-scale micropore alignment in oriented polycrystalline metal−organic framework films via heteroepitaxial growth. *Nat. Mater.* **2017**, *16*, 342−348.
(28) Liu, J.; Qiao, S. Z.; Hartono, S. B.; Lu, G. Q. Monodisperse yolk-shell nanoparticles with a hierarchical porous structure for delivery vehicles and nanoreactors. *Angew. Chem., Int. Ed.* **2010**, *122*, 5101−5105.
(29) Guan, B. Y.; Yu, L.; Lou, X. W. Chemically assisted formation of monolayer colloidosomes on functional particles. *Adv. Mater.* **2016**, *28*, 9596−9601.
(30) Yue, Q.; Li, J.; Zhang, Y.; Cheng, X.; Chen, X.; Pan, P.; Su, J.; Elzatahry, A.; Alghamdi, A.; Deng, Y.; Zhao, D. Plasmolysis-inspired nanoengineering of functional yolk-shell microspheres with magnetic core and mesoporous silica shell. *J. Am. Chem. Soc.* **2017**, *139*, 15486−15493.
(31) Lan, K.; Xia, Y.; Wang, R.; Zhao, Z.; Zhang, W.; Zhang, X.; Elzatahry, A.; Zhao, D. Confined interfacial monomicelle assembly for precisely controlled coating of single-layered titania mesopores. *Matter* **2019**, *1*, 527−538.
(32) Li, Y.; Lu, X. F.; Xi, S.; Luan, D.; Wang, X.; Lou, X. Synthesis of N-doped highly graphitic carbon urchin-like hollow structures loaded with single-Ni atoms towards efficient CO_2 electroreduction. *Angew. Chem., Int. Ed.* **2022**, *61*, No. e2022014.
(33) Zhao, Z.; Duan, L.; Zhao, Y.; Wang, L.; Zhang, J.; Bu, F.; Sun, Z.; Zhang, T.; Liu, M.; Chen, H.; Yang, Y.; Lan, K.; Lv, Z.; Zu, L.; Zhang, P.; Che, R.; Tang, Y.; Chao, D.; Li, W.; Zhao, D. Constructing unique mesoporous carbon superstructures via monomicelle interface confined assembly. *J. Am. Chem. Soc.* **2022**, *144*, 11767−11777.
(34) Han, X.; Zhang, T.; Wang, X.; Zhang, Z.; Li, Y.; Qin, Y.; Wang, B.; Han, A.; Liu, J. Hollow mesoporous atomically dispersed metal-nitrogen-carbon catalysts with enhanced diffusion for catalysis involving larger molecules. *Nat. Commun.* **2022**, *13*, No. 2900.
(35) Imhof, A.; Pine, D. J. Ordered microporous materials by emulsion templating. *Nature* **1997**, *389*, 948−951.
(36) Lin, H.-P.; Cheng, Y.; Mou, C. Hierarchical order in hollow spheres of mesoporous silicates. *Chem. Mater.* **1998**, *10*, 3772−3776.
(37) Gu, D.; Bongard, H.; Deng, Y.; Feng, D.; Wu, Z.; Fang, Y.; Mao, J.; Tu, B.; Schüth, F.; Zhao, D. An aqueous emulsion route to synthesize mesoporous carbon vesicles and their nanocomposites. *Adv. Mater.* **2010**, *22*, 833−837.
(38) Niu, D.; Ma, Z.; Li, Y.; Shi, J. Synthesis of core-shell structured dual-mesoporous silica spheres with tunable pore size and controllable shell thickness. *J. Am. Chem. Soc.* **2010**, *132*, 15144−15147.
(39) Zhao, T.; Wang, X.; Sun, Z.; Wang, H.; Qiu, P.; Xiao, Q.; Jiang, W.; Wang, L.; Bu, F.; Luo, W. Hollow mesoporous metal organic framework single crystals enabled by growth kinetics control for enhanced photocatalysis. *Adv. Funct. Mater.* **2023**, *33*, No. 2303644.
(40) Guan, B. Y.; Yu, L.; Lou, X. W. Formation of Asymmetric Bowl-Like Mesoporous Particles via Emulsion-Induced Interface Anisotropic Assembly. *J. Am. Chem. Soc.* **2016**, *138*, 11306−11311.
(41) Dong, R.; Zheng, L.; Bai, Y.; Ni, Q.; Li, Y.; Wu, F.; Ren, H.; Wu, C. Elucidating the mechanism of fast Na storage kinetics in ether electrolytes for hard carbon anodes. *Adv. Mater.* **2021**, *33*, No. 2008810.
(42) Hou, B. H.; Wang, Y.; Ning, Q.; Li, W.; Xi, X.; Yang, X.; Liang, H.; Feng, X.; Wu, X. Self-supporting, flexible, additive-free and scalable hard carbon paper self-interwoven by one-dimensional microbelts: superb room/low-temperature sodium storage and working mechanism. *Adv. Mater.* **2019**, *31*, No. 1903125.
(43) Liu, Z.; Li, W.; Sheng, W.; Liu, S.; Li, R.; Li, Q.; Li, D.; Yu, S.; Li, M.; Li, Y.; Jia, X. Tunable hierarchically structured meso-macroporous carbon spheres from a solvent-mediated polymerization-induced self-assembly. *J. Am. Chem. Soc.* **2023**, *145*, 5310−5319.
(44) Liu, L.; He, Y.; Yin, S.; Chang, X.; Zhang, J.; Peng, L.; Li, J.; Ma, Y.; Wei, Q.; Lan, K.; Zhao, D. Bimodal ordered porous hierarchies from cooperative soft-hard template pairs. *Matter* **2023**, *6*, 3099−3111.
(45) Wang, B.; Fang, Z.; Jiang, Q.; Tang, D.; Fan, S.; Huang, X.; Li, J.; Peng, D.; Wei, Q. Interlayer confined water enabled pseudocapacitive sodium-ion storage in nonaqueous electrolyte. *ACS Nano* **2024**, *18*, 798−808.
(46) Chen, X.; Tian, J.; Li, P.; Fang, Y.; Fang, Y.; Liang, X.; Feng, J.; Dong, J.; Ai, X.; Yang, H.; Cao, Y. An overall understanding of sodium storage behaviors in hard carbons by an "adsorption-intercalation/filling" hybrid mechanism. *Adv. Energy Mater.* **2022**, *12*, No. 2200886.
(47) Lu, P.; Sun, Y.; Xiang, H.; Liang, X. 3D amorphous carbon with controlled porous and disordered structures as a high-rate anode material for sodium-ion batteries. *Adv. Energy Mater.* **2018**, *8*, No. 1702434.

https://doi.org/10.1021/jacsau.4c00421
JACS Au 2024, 4, 2666−2675